12th International Symposium on Turbulence and Shear Flow Phenomena (TSFP12)
Osaka, Japan, July 19–22, 2022

EFFECT OF THE SURFACE MORPHOLOGY ON ROUGH WALL TURBULENCE

Yoshiki Yamamoto, Shinya Tabata, Yusuke Kuwata*, Kazuhiko Suga
Department of Mechanical Engineering,
Osaka Prefecture University
Sakai, Osaka 599-8531, Japan.
kuwata@me.osakafu-u.ac.jp

ABSTRACT

To clarify the effects of the surface morphology on rough wall turbulence, we conducted experiments on turbulent flows over three-dimensional irregular rough surfaces in which the skewness factor and effective slope were systematically varied. For the rough surface, the root-mean-square roughness was remained fixed while the skewness factor was $Sk = \pm 0.4$, and the effective slope, ES, was varied from 0.09 to 0.72. It is found that the roughness function ΔU^+ for the positively-skewed surfaces ($Sk = +0.4$) is larger than that for the negatively-skewed surfaces ($Sk = -0.4$), and ΔU^+ increases with increasing the effective slope. The transitional behavior to the fully rough regime strongly depends on ES but not on Sk: the steep surfaces tend to lead to a sudden transition to the fully rough regime, whereas the transitional behavior for the wavy surfaces with the small ES value is close to the Colebrook-type transition. The equivalent sand-grain roughness linearly increases with increasing the ES value from 0.09 to 0.36, while the increasing trend slows down when the ES value further increases. It is also found that the effects of the skewness factor on the equivalent sand-grain roughness do not largely depend on the ES values.

Background

Surfaces in engineering systems typically have roughness, and cannot be regarded as hydraulically smooth, particularly for high Reynolds number flows. Familiar examples include a surface of a turbine blade in harsh operating conditions and a surface with deposition of incombustible ash in internal combustion engines. It is well established that in the fully rough regime where wall roughness protrudes into the logarithmic region, a downward shift value in the inner-scaled mean velocity ΔU^+ follows a universally-accepted correlation (Flack & Schultz, 2010):

$$B - \Delta U^+ + \frac{1}{\kappa}\ln(k_s^+) = 8.5, \quad (1)$$

where κ is the von Kármán constant, B is the log-law intercept for smooth wall turbulence, and k_s^+ is the inner-scaled equivalent sand-grain roughness. The correlation suggests that in the fully rough regime, the effect of wall roughness on the mean velocity can be predicted once we obtain k_s for the rough surface of interest. However, there is still no universal correlation that estimates k_s from morphological information of the rough surface. In addition, a further difficulty arises in predicting the effects of wall roughness on ΔU^+ in the transitionally rough regime, because ΔU^+ in this regime depends not only on k_s but also on the other parameters (Flack & Schultz, 2010; Flack *et al.*, 2012). The effects of the surface morphology on the roughness function or the equivalent sand-grain roughness have been extensively studied. One of the well-known important parameters that have a large impact on the roughness effect is the skewness factor Sk, which is defined as the statistical moment of the surface elevation. Flack & Schultz (2010); Forooghi *et al.* (2017); Kuwata & Kawaguchi (2019); Kuwata & Nagura (2020) showed that the surfaces with the positive skewness yield larger frictional resistance. Another well-studied parameter is the effect slope, which quantifies the steepness of the surface undulations (Napoli *et al.*, 2008). The recent direct numerical simulation (DNS) study by (Ma *et al.*, 2020) showed that ΔU^+ can be expressed as a function of a new coupling scale ESk^+, which is a product of the effective slope ES and the roughness height k:

$$\Delta U^+ = 2.66[\log(ESk^+] + C, \quad (2)$$

where $C = 1.46$ is adopted for the three-dimensional sinusoidal rough walls. However, it is still unclear on the combined effects of those parameters, and this motives us to examine the effects of ES and Sk on the rough wall turbulence from the transitionally rough to fully rough regimes. In this study, we focus on the two typical morphological parameters of rough surfaces, namely the skewness factor Sk and effective slope ES, and we aim to clear the effect of Sk and ES from the transitionally rough regime to the fully rough regime.

Experimental methods

Experiments were conducted in the rectangular duct with a bottom rough surface. A sketch depicting the experimental facility is provided in Figure 1. Tap water from a header tank goes into a flow straightener where the flow is conditioned by honeycomb-bundled, and the fluid temperature was recorded by a digital thermometer (FD-T1, Keyence). The conditioned flow develops in the upstream portion of the rectangular duct whose cross-section is 50mm in height (H), and 400mm in width (W). This gives the aspect ratio of $W/H = 8$ which is sufficient to assume that the flow is two-dimensional in the middle of the duct. The duct consisted of smooth acrylic

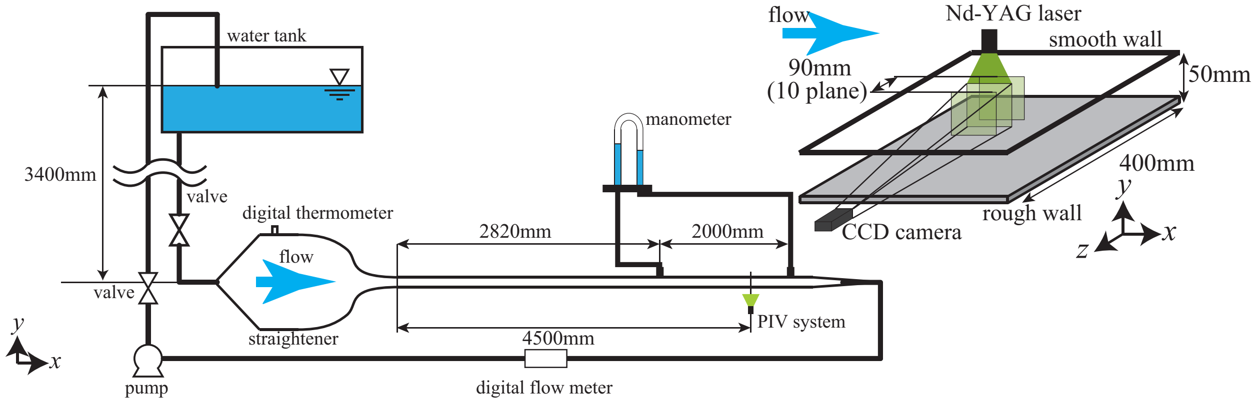

Figure 1. Experimental apparatus.

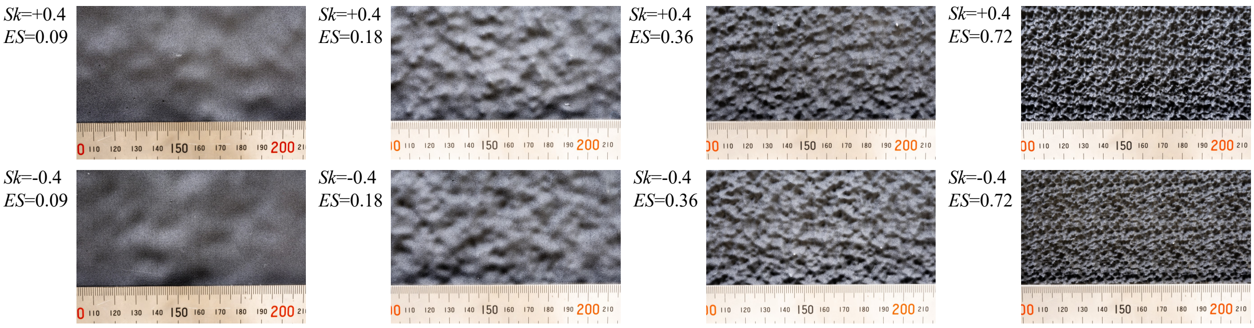

Figure 2. Three-dimensional irregular rough surfaces with the *Sk* and *ES* values.

walls, and a rough surface was considered for the bottom of the duct. The fully developed turbulent flow was measured at 4.5 m (90H) from the duct entrance. A pressure difference was measured by a U-tube manometer with pressure taps along the centerline of the top wall. The pressure taps were spaced 2m apart, and the tap in the upstream position was located at 2.8m (56H) from the duct entrance. The flow rate was controlled by the pump with the power converter and adjusted such that the bulk Reynolds number was close to the target value in the range of $Re = 2,000$ to $45,000$. Here, the Reynolds number is defined as $Re = U_b(H - k_m)/\nu$ where k_m is the mean surface height, and U_b is the bulk mean velocity.

The flow properties were measured by a two-component PIV system, which consists of a dual pulsed Nd-YAG laser delivering 532 nm beams with pulse energy of 70 MJ (EverGreen, Quantel), CCD camera of 20.4 fps (FlowSense EO 4M, Dantec Dynamics), the camera lens of Micro-Nikkor 55 mm f/2.8 (Nikon) and computer for data acquisition. A single recorded frame covers the zone of $50 \times 50\text{mm}^2$ with 2080×2080 pixel. The nylon powder (Kanomax) was used for the tracer particle, and the seeding density was adjusted to obtain more than 30 particle-image pairs in each interrogation window whose size was set to 32×32 pixel. Each image was processed to produce 127×127 vectors from the interrogation windows. The image sampling rate is 5Hz (the statistical time is almost 200s) and 1000 image pairs are processed in this study. As the rough surfaces used in this study are three-dimensional irregular rough surfaces, the mean profiles above the rough surfaces are inhomogeneous in the streamwise and spanwise directions. Therefore, to obtain the spatial and Reynolds averaged profiles above the rough surfaces, we measured 10 $x-y$ planes with an offset of 10mm intervals from a center plane, and an ensemble-averaged value is also averaged over 10 $x-y$ planes.

Rough surface

In this study, we considered 8 rough surfaces in which the Sk and ES values were systematically varied while the root-mean-square roughness remained fixed: $k_{rms} = 0.85$mm. The root-mean-square roughness k_{rms} represents the variance from the mean surface height k_m, which is defined as follows:

$$k_{rms}^2 = \frac{1}{L_x L_z} \int_x \int_z (h(x,z) - k_m)^2 \, dxdz, \quad (3)$$

where L_x and L_z respectively denote the streamwise and spanwise lengths of the rough surface, and $h(x,z)$ is the surface height. Here, the mean surface height k_m is given as follows:

$$k_m = \frac{1}{L_x L_z} \int_x \int_z (h(x,z)) \, dxdz. \quad (4)$$

The skewness factor Sk quantifies the asymmetry of the probability density function of the roughness height elevation, which is defined as follows:

$$Sk = \frac{1}{k_{rms}^3 L_x L_z} \int_x \int_z (h(x,z) - k_m)^3 \, dxdz. \quad (5)$$

The effective slope ES represents the steepness of the rough surface undulation, which is defined as follows:

$$ES = \frac{1}{L_x L_z} \int_x \int_z \left| \frac{\partial h(x,z)}{\partial x} \right| dxdz. \quad (6)$$

We numerically generated the original surface with $ES = 0.09$ and $Sk = +0.4$, by superimposing differently sized hyperbolic shape roughness elements (Kuwata & Nagura, 2020). Based on the original rough surface, we changed the sign of *Sk* by inverting the surface height, whereas the *ES* value was increased by reducing the surface width in the streamwise and spanwise directions while preserving the surface height. The numerically generated 8 rough surfaces were duplicated by a 3D printer as shown in Figure 2, in which the *ES* value ranges from 0.09 to 0.72, and the *Sk* value takes either of the values -0.4 or $+0.4$.

Results and discussions

Figure 3 shows the inner-scaled mean velocity profiles for the surfaces with $ES = 0.36$ at $Re \approx 2.0 \times 10^3, 4.0 \times 10^3$, and 1.5×10^4 together with the smooth wall profile at $Re \approx 4.1 \times 10^4$ (Kawamura, 2008). Here, the normal distance from the mean surface location k_m is used as the distance from the rough surface. The figure confirms that the mean velocity profiles over the rough surface are considerably lower than the smooth wall profile, while the profiles seem to maintain the logarithmic profile away from the rough walls. The downward shift value from the smooth wall profile, which is referred to as the roughness function ΔU^+, is 11.9 for the positively-skewed surface ($Sk = +0.4$) at $Re \approx 1.5 \times 10^4$ in Fig.3(a), while it is 9.9 for the negatively-skewed surface ($Sk = -0.4$) at the same Reynolds number in Fig.3(b). That is, ΔU^+ for the positively-skewed surfaces is larger than that for the negatively-skewed surfaces. We also observe that the ΔU^+ progressively increases with increasing *Re*. Given that the roughness function measures an increase in the skin friction coefficient, the figure confirms that the positively-skewed surfaces yield larger friction resistance compared with the negatively-skewed surfaces. This is consistent with the previous experimental and DNS studies (Flack & Schultz, 2010; Forooghi *et al.*, 2017; Kuwata & Kawaguchi, 2019; Kuwata & Nagura, 2020).

Figure 4 shows the mean velocity profile in velocity-defect form for the surfaces with $ES = 0.36$ together with the smooth wall profiles at $Re \approx 3.2 \times 10^3$ (Iwamoto *et al.*, 2002) and $Re \approx 4.1 \times 10^4$ (Kawamura, 2008). Here, U_δ^+ denotes the maximum peak value of U^+, and δ is the boundary layer thickness for the rough wall side, which is computed as the distance from the mean surface height to the maximum velocity location. The figure confirms that for the cases with $Sk = +0.4$ and $Sk = -0.4$, the mean velocity profile in the velocity-defect form shows similarity to some extent for the cases. However, the Reynolds number dependence on the mean velocity defect is not consistent with the smooth wall cases. The possible explanation is the effects of the top smooth wall. The flows for smooth wall cases are bounded by two parallel smooth walls, whereas the flows in the present experiments are bounded by the top smooth and bottom rough walls. Hence, the top smooth wall may affect the mean velocity profiles on the rough wall side.

To better understand the Reynolds number dependence of the roughness function, we focus on the behavior of ΔU^+ against k_s^+ in Figure 5. The solid line shows the experimental result for the sand-grain surface by Nikuradse (Nikuradse, 1933), and the broken line shows the experimental result for the wavy surface by Colebrook (Colebrook, 1939). Here, the equivalent sand-grain roughness k_s is determined from Eq.(1). Fig.5(a) clearly confirms that ΔU^+ in the fully rough regime depends solely on k_s^+, whereas the transitional behavior to the fully rough regime significantly differs depending on the surface geometry. The same trend can be observed for the negatively-skewed surfaces in Fig.5(b). In Fig.5 (a,b), it is

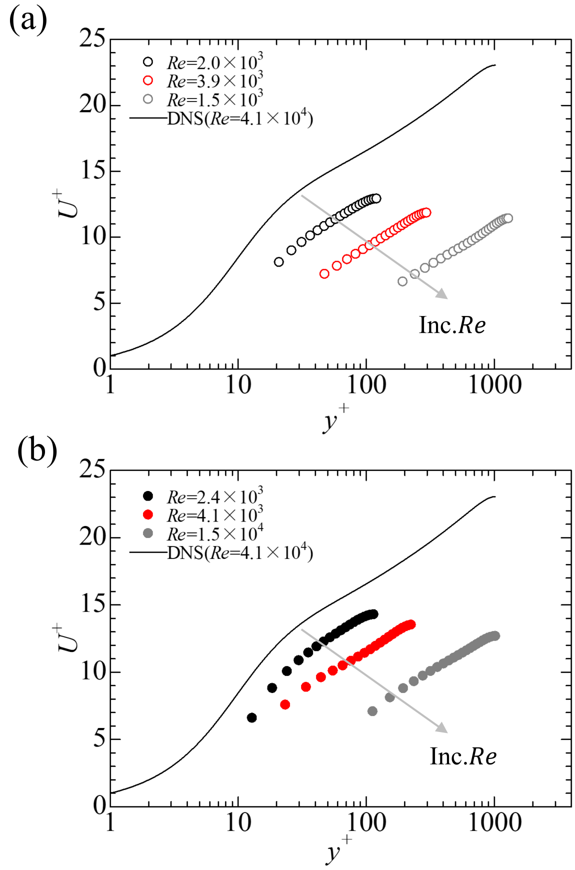

Figure 3. Inner-scaled streamwise mean velocity profiles at different bulk mean Reynolds numbers for $ES = 0.36$: (a)$Sk = +0.4$ and (b)$Sk = -0.4$. The DNS data for smooth wall case by (Kawamura, 2008) is included for comparison.

found that ΔU^+ for the steep rough surfaces with $ES = 0.36$ and 0.72 exhibits a sudden transition to the fully rough regime, and the onset of the fully rough regime is delayed in comparison with the asymptote for the sand-grain by Nikuradse (Nikuradse, 1933). For the case with $ES = 0.18$, the asymptotic behavior of ΔU^+ is close to the Nikuradse-type transition. For the wavy surface with $ES = 0.09$, the asymptotic behavior of ΔU^+ is the most moderate and close to the Colebrook-type transition (Colebrook, 1939). Therefore, it is conceivable that the asymptotic behavior to the fully rough regime depends on the steepness of the rough surfaces but not on the skewness factor.

To see the Reynolds number dependence of the turbulence intensities, Figure 6 shows the profiles of the streamwise and wall-normal root-mean-square velocity fluctuations for the case with $ES = 0.36$ and $Sk = +0.4$. For comparison, the DNS data from Kawamura (2008); Iwamoto *et al.* (2002) are included. The figure confirms that the profiles of u_{rms}^+ and v_{rms}^+ near the rough surfaces deviate largely from the smooth wall profiles, whereas those away from the rough surfaces are rather close to the DNS data irrespective of the Reynolds number. For the streamwise component, the maximum peak value of u_{rms}^+ is significantly reduced by the wall roughness, and the maximum peak value decreases with increasing the Reynolds number. In contrast, for the wall-normal component, the maximum peak value of v_{rms}^+ increases with increasing the Reynolds number. This trend is consistent with the experimental studies (Flack *et al.*, 2007; Flack & Schultz, 2014) and DNS studies (Forooghi *et al.*, 2018; Kuwata & Kawaguchi, 2019). It

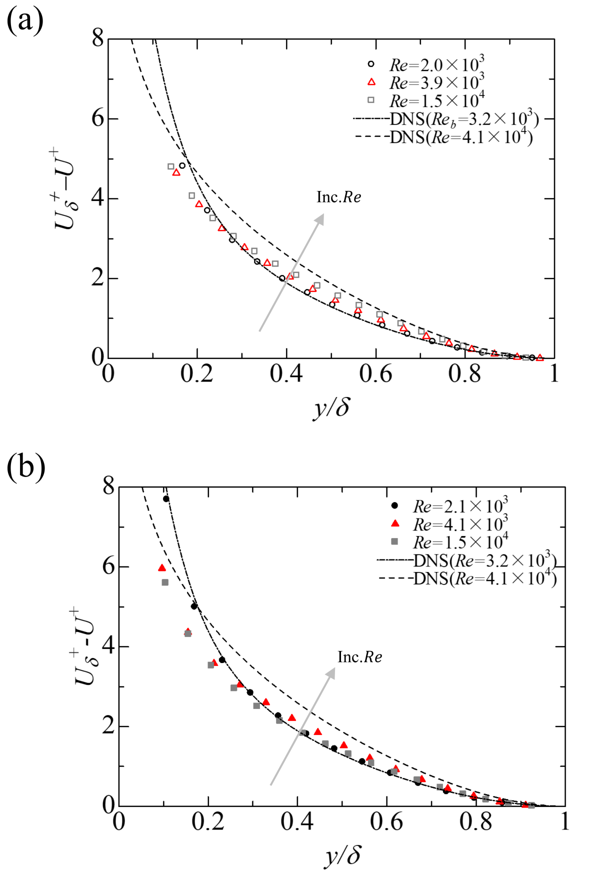

Figure 4. Mean velocity profile in velocity-defect form at different bulk mean Reynolds numbers for $ES = 0.36$: (a)$Sk = +0.4$ and (b)$Sk = -0.4$. For comparison, the DNS data from Kawamura (2008); Iwamoto *et al.* (2002) are included.

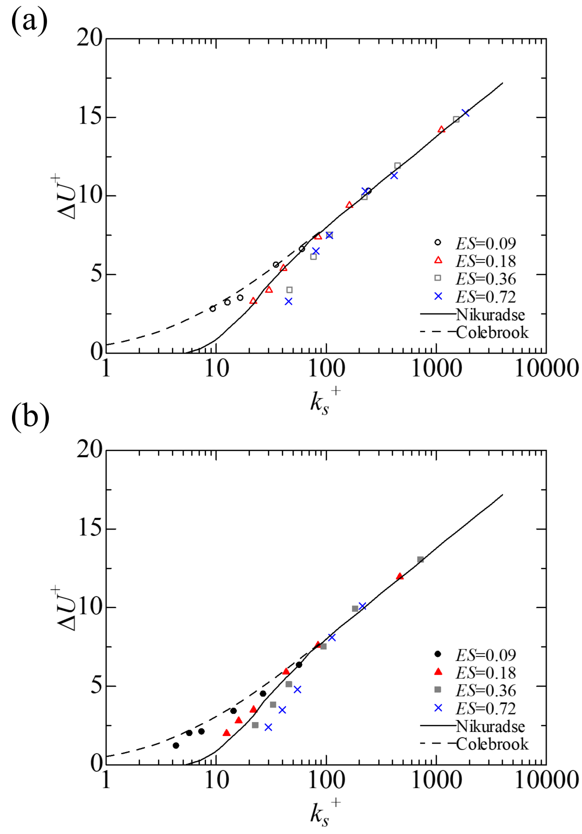

Figure 5. Roughness function ΔU^+ against the inner-scaled equivalent sand-grain roughness k_s^+ together with the correlations from (Nikuradse, 1933; Colebrook, 1939): (a)$Sk = +0.4$ and (b)$Sk = -0.4$.

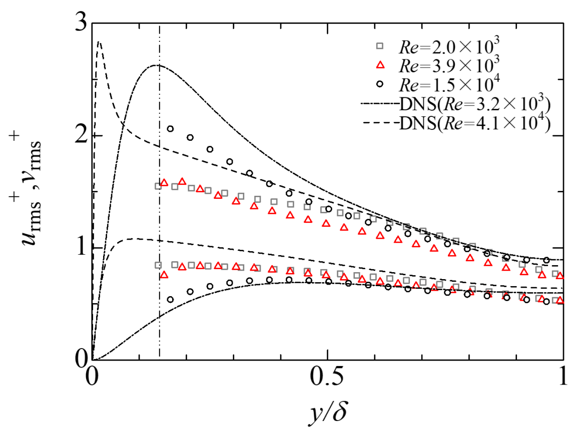

Figure 6. Comparison of the streamwise and wall-normal turbulence intensities at different bulk mean Reynolds numbers together with the DNS data from Kawamura (2008); Iwamoto *et al.* (2002). The position of the maximum roughness crest is denoted by the broken line in the figure.

is also suggested that the turbulence near the porous wall tends to be more isotropic as the Reynolds number increases.

The effects of the steepness on the turbulence intensities are shown in Figure 7 where the profiles of the streamwise and wall-normal turbulence intensities for the cases with $Sk = +0.4$ at the Reynolds number of $Re \simeq 4000$ are shown. We observe that the profiles of u^+_{rms} and v^+_{rms} away from the rough surfaces are close to each other, whereas the effects of the ES values are clearly visible near the rough surfaces. As the ES value increases, the maximum peak value of u^+_{rms} tends to decrease but v^+_{rms} tends to increase. Although the results are not shown here, the effect of the steepness is consistent for the other Reynolds number cases and the negatively-skewed rough surface cases.

To better understand the effect of Sk and ES on the equivalent sand-grain roughness, Figure8 displays k_s/k_{rms} for all rough surface cases. The first notable observation is that the k_s/k_{rms} value increases with the ES value, and the k_s value for the positively-skewed surface is consistently larger than that for the negatively-skewed surface. The effects of the ES and Sk values are in line with the earlier findings by Napoli *et al.* (2008); Chan *et al.* (2015); Kuwata & Kawaguchi (2019); Flack *et al.* (2020); Kuwata & Nagura (2020). Interestingly, the k_s value for $Sk = +0.4$ is approximately 1.7 times larger than that for $Sk = -0.4$ irrespective of the ES value. This increase ratio roughly corresponds to the value of 2.4 obtained by the correlations of $k_s/k_{rms} = 2.48(1+Sk)^{2.24}(Sk > 0)$ and $k_s/k_{rms} = 2.73(2+Sk)^{-0.45}(Sk < 0)$ proposed by Flack *et al.* (2020), and 1.7 from the correlation of $k_s/k_{rms} = 4.0(1 + 0.17Sk)^4$ proposed by Kuwata & Kawaguchi (2019). The other important findings from Fig.8 is that the k_s/k_{rms} value linearly increases with the ES value when $ES \leq 0.36$, while the increase ratio shows down when the ES value further increases. The similar observation was found by (Ma *et al.*, 2020) who showed that the roughness length scale multiplied by ES well correlates with the roughness function. This suggests that

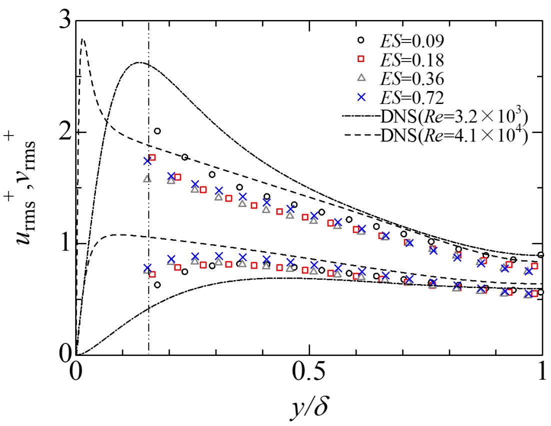

Figure 7. Effects of the effective slope on the streamwise and wall-normal turbulence intensities together with the DNS data from Kawamura (2008). The position of the maximum roughness crest is denoted by the broken line in the figure

when the ES value is moderate ($ES < 0.4$), the roughness length scale multiplied by the ES value, e.g., ESk_{rms}, may be one of the candidates for predicting the equivalent sand-grain roughness.

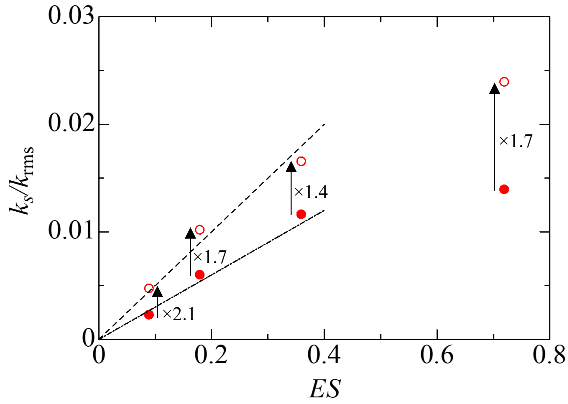

Figure 8. Effects of the ES and Sk values on the equivalent sand-grain roughness. The ratio of the k_s/k_{rms} for $Sk = +0.4$ to that for $Sk = -0.4$ is also shown.

Finally, we discuss the other parametrization for ΔU^+ with the wall-normal velocity fluctuations. Orlandi *et al.* (2006); Orland & Leonardi (2008) reported that the effects of the wall roughness are strongly connected with the wall-normal velocity disturbances, and the roughness function can be reasonably predicted by the wall-normal turbulence intensity:

$$\Delta U^+ = (B/\kappa)v^+_{rms}, \quad (7)$$

where B is a log-law intercept for smooth wall, and κ is the von Kármán constant. To investigate the correlation between ΔU^+ against v^+_{rms}, Figure 9 presents a variation of ΔU^+ against v^+_{rms} at the roughness crest. We can see the correlation between ΔU^+ against v^+_{rms}. However, the experimental data are significantly scattered and do not show the qualitative agreement with Eq.(7). Moreover, we can observe that the linear relation between ΔU^+ against v^+_{rms} does not hold when $v^+_{rms} > 0.9$. The reason is not clear; however, the discrepancy with the correlation of Eq.(7) may be attributed to differences in the flow conditions and rough surface geometry with those by Orlandi *et al.* (2006); Orland & Leonardi (2008).

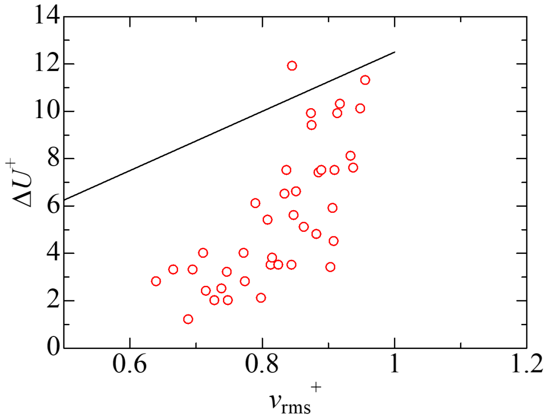

Figure 9. Variation of ΔU^+ against v^+_{rms} at the roughness crest.

CONCLUSION

We performed the PIV measurements for three-dimensional irregular rough surfaces in which the skewness factor and effective slope were systematically varied to clarify the effects of the surface morphology on the frictional resistance. For the present rough surface, the root-mean-square roughness height was fixed, while the skewness factor was $Sk = \pm 0.4$, and the effective slope, ES, was varied from 0.09 to 0.72. We discuss the effects of ES and Sk on the transitional behavior to the fully rough regime. It is revealed that the transition to the fully rough regime becomes steeper as ES increases, and the transitional behavior does not depend on the skewness factor Sk. Discussion on the effects of ES and Sk on the equivalent sand-grain roughness shows that the equivalent sand-grain roughness for the surfaces with $Sk = +0.4$ is consistently larger than that for $Sk = -0.4$, and the increase ratio does not strongly depend on the ES value. It is also found that the equivalent sand-grain roughness linearly increases with the ES value, while the increase ratio slows down for the steep rough surfaces with $ES > 0.36$, suggesting that the product of the roughness length scale k_{rms} and ES can be used for predicting the equivalent sand-grain roughness when the ES value is moderate ($ES \leq 0.36$).

REFERENCES

Chan, L., MacDonald, M., Chung, D., Hutchins, N. & Ooi, A. 2015 A systematic investigation of roughness height and wavelength in turbulent pipe flow in the transitionally rough regime. *J. Fluid Mech.* **771**, 743–777.

Colebrook, C.F. 1939 Turbulent flow in pipes with particular reference to the transitional region between smooth and rough pipe laws. *Journal of the Institution of Civil Engineers* **12**, 393–422.

Flack, K.A & Schultz, M.P 2010 Review of hydraulic roughness scales in the fully rough regime. *J. Fluids Eng.* **132** (4).

Flack, K.A & Schultz, M.P. 2014 Roughness effects on wall-bounded turbulent flows. *Phys.Fluids* **26**, 101305.

Flack, K.A., Schultz, M.P. & Barros, J.M. 2020 Skin friction measurements of systematically-varied roughness: probing the role of roughness amplitude and skewness. *Flow Turb. Combust.* **104** (2), 317–329.

Flack, K.A., Schultz, M.P. & Connelly, J. 2007 Examination of a critical roughness height for outer layer similarity. *Phys. Fluids* **19**, 095104.

Flack, K.A, Schultz, M.P. & Rose, W.B. 2012 The onset of roughness effects in the transitionally rough regime. *Int. J. Heat Fluid Flow* **35**, 160–167.

Forooghi, P., Stroh, A., Magagnato, F., Jakirlić, S. & Frohnapfel, B. 2017 Toward a universal roughness correlation. *J. Fluids Eng.* **139** (12).

Forooghi, P., Stroh, A., Schlatter, P. & Frohnapfel, B. 2018 Direct numerical simulation of flow over dissimilar, randomly distributed roughness elements: A systematic study on the effect of surface morphology on turbulence. *Phys. Rev. Fluid* **3**, 044605.

Iwamoto, K., Suzuki, Y. & Kasagi, N. 2002 Database of fully developed channel flow. `http://www.thtlab.t.u-tokyo.ac.jp/index-j.html`.

Kawamura, H. 2008 Direct numerical simulation database for turbulent channel flow with heat transfer. `https://www.rs.tus.ac.jp/t2lab/db/`.

Kuwata, Y. & Kawaguchi, Y. 2019 Direct numerical simulation of turbulence over systematically varied irregular rough surfaces. *J.Fluid Mech.* **862**, 781–815.

Kuwata, Y. & Nagura, R. 2020 Direct numerical simulation on the effects of surface slope and skewness on rough-wall turbulence. *Phys. Fluids* **32** (10), 105113.

Ma, G.-Z., Xu, C.-X., Sung, H.J. & Huang, W.-X. 2020 Scaling of rough-wall turbulence by the roughness height and steepness. *J. Fluid Mech.* **900**.

Napoli, E., Armenio, V. & De Marchis, M. 2008 The effect of the slope of irregularly distributed roughness elements on turbulent wall-bounded flows. *J. Fluid Mech.* **613**, 385–394.

Nikuradse, J. 1933 Laws of flow in rough pipes. *National Advisory Committee for Aeronautics* .

Orland, P. & Leonardi, S. 2008 Direct numerical simulation of three-dimensional turbulent rough channels: parameterization and flow physics. *J. Fluid Mech.* **606**.

Orlandi, P., Leonardi, S. & Antonia, R.A. 2006 Turbulent channel flow with either transverse or longitudinal roughness elements on one wall. *J. Fluid Mech.* **561**, 279–305.